



Confirmation of the healing mechanism in a mendable EMAA–epoxy resin

Samuel Meure, Russell J. Varley^{*}, Dong Yang Wu, Sherri Mayo, Kate Nairn, Scott Furman

CSIRO Materials Science and Engineering, Clayton South, Vic. 3168, Australia

ARTICLE INFO

Article history:

Received 16 May 2011

Received in revised form 26 November 2011

Accepted 29 November 2011

Available online 8 December 2011

Keywords:

Polymers
Fracture
Toughness
Healing

ABSTRACT

The healing of a mendable epoxy resin containing polyethylene-*co*-methacrylic acid (EMAA) particles has been confirmed to occur via a pressure delivery mechanism of the healing agent, EMAA, into a crack plane during thermal activation. Internal pressure rises within a bubble, formed from interactions between EMAA particles causing expansion of the bubble which subsequently force the healing agent to flow into an available cavity. The use of X-ray ultra-microscopy (Xum), scanning electron microscopy (SEM) and energy dispersive spectroscopy (EDS) provides evidence for volatile formation, bubble expansion and delivery of healing agent. Spectroscopic studies of the interfacial reactions between epoxy and EMAA during post-cure, compared with adhesion and fracture toughness measurements, reveal that hydroxyl acid reactions catalysed via tertiary amine initiate the pressure delivery mechanism. Furthermore, adhesion and FTIR measurements suggest that the re-binding or healing of a crack interface is likely to be dominated by hydrogen bonding.

Crown Copyright © 2011 Published by Elsevier Ltd. All rights reserved.

1. Introduction

Self healing polymers and mendable polymers have been proposed as a method of improving the durability of brittle polymers and polymer composites used in structural applications [1–5]. Self-healing polymers are typified by the microcapsule-based [6–10] and hollow fibre-based [11–15] systems which autonomically repair damage through the re-binding of fracture surfaces during solidification of polymerizable healing agents. These self-healing systems can completely eliminate the need for manual intervention during repair but typically require the encapsulation of multiple reagents within the bulk phase which can be expensive, difficult to produce or possess a limited lifespan. In contrast to these self-healing polymers, mendable polymers are typified by resins containing reversible Diels–Alder [16–20] crosslinks or the thermoplastic-thermoset solid solutions [1,21] which repair damage after external stimuli (such as heat) have been applied to the damaged material. Similar levels of repair can be achieved

in both the self-healing and mendable polymers; however the need for external stimuli during healing of the mendable polymers has enabled the use of cheap and stable materials as healing agents. Two examples of cheap and stable mendable polymer healing agents include the polybisphenol-A-*co*-epichlorohydrin used by Hayes et al. [21] and polyethylene-*co*-methacrylic acid (EMAA) used by Meure et al. [22].

This paper focuses on polyethylene-*co*-methacrylic acid (EMAA), a relatively new type of thermally activated healing agent use to produce mendable epoxy resins. Although the performance of EMAA healing agents as resin preparation and healing conditions are varied [23] and the binding mechanism between EMAA and the resin [24] have been reported; a better understanding of the actual healing mechanism proposed by Meure et al. is required. Initially, the EMAA particles are added to the resin and bind with the epoxy resins within the polymer network during curing. It was then proposed that post curing of the resin resulted in the formation of small bubbles within the discrete EMAA particles. During fracture, these particles were shown to fracture during crack growth; producing a surface that possessed resin-rich and EMAA-rich regions. When the damaged resin was heated to 150 °C, it was

^{*} Corresponding author. Tel.: +61 3 9545 2941; fax: +61 3 9544 1128.

E-mail address: russell.varley@csiro.au (R.J. Varley).

proposed that the EMAA was forced into the fracture plane by the expansion of the small bubbles. The flow of EMAA into the fracture plane would then facilitate healing by EMAA as the particles rebind together the adjacent epoxy fracture surfaces. Healing or healing efficiency based upon this technology refers to the extent to which adhesion between fractured interfaces is restored with respect to the original failure. Previous studies with EMAA as a healing agent in epoxy amine systems have shown that over 100% healing can be achieved for both the polymer networks [22] and the carbon fibre reinforced composite [25].

In this study, the phase compositions and binding reactions between the epoxy/amine resins during healing are investigated to provide a better understanding of the pressure delivery healing mechanism. The internal structure of the mendable resins is assessed using X-ray ultra-microscopy (Xum) and scanning electron microscopy (SEM) in conjunction with energy dispersive spectra (EDS) to confirm the presence of discrete EMAA particles possessing small bubbles after healing. The chemistry associated with healing in the mendable resins is then investigated using near infrared (NIR), attenuated total reflectance Fourier transformed infrared (ATR-FTIR) and nuclear magnetic resonance (NMR). In conjunction with understanding the chemistry, the mechanical and healing properties were characterised by measuring the adhesive strength of epoxy butt joints and the repair capability in single edge notched beam bending (SENB) testing. In this way, the mendable resins internal structure and healing chemistry will have been confirmed and provide further insight into the solid state EMAA healing mechanism.

2. Experimental procedures

2.1. Sample preparation

Epoxy butt joint test pieces were produced by curing a diglycidyl ether of bis-phenol A epoxy resin, (DGEBA, DER-331, Dow Plastics Australia) with tri-ethyl tetramine (TETA, DEH-24, Dow Plastics Australia) in a 1:1 stoichiometric formulation. These resins were then cured in silicone moulds for 2 h at 30 °C then post cured at 150 °C for designated times ranging between 0 and 90 min. EMAA films (Nucler 2940, DuPont Packaging and Industrial Polymers) were produced by pressing at 1000 kPa and 130 °C for 1 min. After pressing, the approximately 130 µm thick EMAA films were dried in a 50 °C oven for 6 days and then stored in a desiccator. Butt joints were produced by heat treating a 16 mm diameter EMAA film sandwiched between two epoxy butt joint test pieces. Initially the EMAA film was adhered to the face of one epoxy butt joint test piece in a 150 °C oven for 7.5 min. A second epoxy butt joint test piece was then pressed on top of the hot EMAA film and stored in the 150 °C oven for a further 22.5 min. After being in the 150 °C oven for a total of 30 min, the test piece was removed from the oven, pressed to further remove any remaining bubbles and then stored in a desiccator.

SENB samples were prepared by curing DGEBA and TETA of varying epoxy: amine stoichiometries typically cured at 50 °C for 90 min in silicone moulds. Stoichiome-

tries ratios were set at 1:1.25, 1:1, 1:0.75, 1:0.5 and 1:0.25 and to adjust for varying reaction kinetics, were post-cured at 30 min at 150 °C, 30 min at 80 °C then 30 min at 150 °C, 45 min at 80 °C then 30 min at 100 °C then 30 min at 150 °C and 45 min at 80 °C then overnight at 100 °C then 30 min at 150 °C, respectively. The EMAA healing agent was cryogenically ground, flushed through a stack of 35 mesh and 60 mesh sieves and then dried under vacuum at 50 °C for 4 days prior to addition to the epoxy resin. Mendable resins were produced by heating the DGEBA to 70 °C, stirring in 15 vol.% EMAA particles and then adding the specified TETA component.

2.2. Imaging

Samples for X-ray ultra-microscopy (Xum) were prepared from sections of SENB using a diamond saw and then sanded into an approximately 10 mm long cylinder with a 2 mm diameter. X-ray microscopy and micro-tomography were carried out using a prototype [26] X-ray ultra-microscope. The instrument is hosted on an SEM to which it adds X-ray microscopy and micro-tomography functionality. A very small X-ray source of size 0.1 µm is generated by focusing the SEM electron beam on a metal target. The sample is placed between the X-ray source and an X-ray CCD detector, giving a point-projection geometry with natural magnification.

For tomography of the healed polymer a Ta foil X-ray target was used with an SEM accelerating voltage of 25 kV. This produces polychromatic X-rays with an average detected X-ray energy constrained by the source characteristics and the detector sensitivity to around 8 keV. Tomographic datasets consisted of 720 views of the sample with 0.5° rotations of the sample between each view. Acquisition time for a single view was of the order of a minute requiring several hours for a full dataset. X-TRACT software [27] was used to process and to produce a 3D reconstruction of the sample from the data. For the initial data the total field of view was approximately 2.6 mm. The higher magnification dataset has a 1.5 mm field of view and a voxel size of 1.15 µm.

Prior to tomographic reconstruction, phase-retrieval methods were used to transform the phase-contrast images to a form more suited as input to a tomographic reconstruction algorithm by, applying Paganin's 'homogeneous' phase-retrieval algorithm [28].

The SEM and EDS results were obtained using a Philips XL30 Field Emission scanning electron microscopy. Prior to imaging at 5 kV, all samples were coated with 200–250 Å of iridium. The EDS point scans and line scan were collected at 10 kV using a LinkISIS EDS System from Oxford Instruments.

2.3. Spectroscopy

Transmission near infra-red spectroscopy (NIR) was performed on SENB samples using a Cary UV-Vis-NIR spectrophotometer. Scans between from 4800–9900 cm⁻¹ were corrected using a shifting baseline, smoothed using an 11 point smoothing function and then normalised according to the 5980 cm⁻¹ peak as an internal standard.

A Bruker Equinox 55 FTIR was used in ATR mode to collect mid FTIR spectra from 600–4000 cm^{-1} . Spectra were averaged over 64 individual scans and the spectra were normalized according to the 1610 cm^{-1} peak. FTIR samples were cut from the surface of butt joints using a diamond saw after the specified heat treatment.

The NMR samples were cryogenically ground into a fine powder prior to analysis. NMR spectra were measured on a Bruker Avance 400, operating at 9.1 T, using a 4 mm Bruker MAS probe with a spin speed of 10 kHz, a 2 ms contact time and a 5 s recycle delay. An external TMS reference was used.

2.4. Mechanical testing

Adhesion tests were carried out on an Instron 5566 machine at 127 mm/min in general accordance with ASTM D897. Typically 10 replicates were used to determine the average adhesive strength and errors were calculated from the standard deviation divided by the square root of the number of joints tested.

SENB testing was carried out in general accordance with ASTM-D5045 using $5 \times 10 \times 50$ mm bars in a 40 mm span three point bend and a crosshead speed of 165 $\mu\text{m s}^{-1}$. A sharp crack was generated in each SENB using a diamond saw to cut a 3 mm deep notch and then tapping carefully with a razor blade to generate a 2 mm deep pre-crack. For the virgin (pre-cracked) material, SENB were loaded until 90% loss of the peak load was reached. Healing was conducted by positioning the SENB notch side up in an oven at 150 $^{\circ}\text{C}$ for 30 min. Re-loading of the healed SENB was carried out using the same procedure as for the virgin SENB but loading was stopped at 99% loss of the peak load. Peak load values were averaged over five test pieces and the standard error was set as the standard deviation in peak load divided by the square root of the number of peak load values recorded.

3. Results and discussion

3.1. Confirmation of the mendable polymer morphology

A Xum image of the mendable polymer morphology is shown in Fig. 1A. Xum differentiates chemical structures on the basis of density, so the lower density of EMAA

compared to the epoxy resin (0.94 and 1.1 g/cm^3 , respectively) illustrates clearly the dispersed EMAA particles within the continuous epoxy matrix. A secondary observation is the appearance of bubbles exclusively in the EMAA particles which provides experimental evidence for the previously proposed healing mechanism.

Xum images further reveal the presence of EMAA in the crack between adjacent fracture surfaces after healing. Two examples where EMAA has been delivered into a horizontal crack from adjacent thermoplastic reservoirs are shown in Fig. 1B and C. The first example in Fig. 1B shows a horizontal line of material with a similar density to the EMAA particles completely filling the cavity. The second example, Fig. 1C shows a similar healing event, but a black region in the middle of the crack, indicative of a very low density region similar to the bubbles observed within the EMAA particles, is attributed to incomplete rejoining by EMAA. Even though the crack and changes in density of the area inside the crack are visible, the dimensions of the crack are approaching the limits of resolution in these images and so further evidence is required in order to confirm the presence of EMAA within the crack after healing.

Potassium hydroxide staining and energy dispersive spectra (EDS) were used to enable better differentiation between the EMAA-rich and resin-rich phases in the healed resins. In order to visualise the healed resin repair morphology, a healed SENB was cross-sectioned perpendicular to the fracture plane and polished at 200 rpm using Kemet Diamond Compound 3-FD-C4. The polished cross-section was then soaked in potassium hydroxide over night such that the potassium ions would form a salt with acid groups in the EMAA [29]. The formation of potassium salts in the EMAA would then mean that the EDS-based detection of potassium could be used to reflect the presence of EMAA in the polished cross-section.

Imaging of the cross-section (cut perpendicular to the damage plane) of the resin revealed discrete particles containing circular voids (formally bubbles) inside, as shown as an example in Fig. 2A. A higher magnification image of the particle–resin interface near the crack (Fig. 2B) was scanned using EDS to reveal the presence of potassium inside the particle (Area 2 – Fig. 2D) but not in the bulk phase (Area 1 – Fig. 2C). This confirmed that EMAA was present as a discrete particle phase in the mendable resin. Further to confirmation that the EMAA remained as a discrete

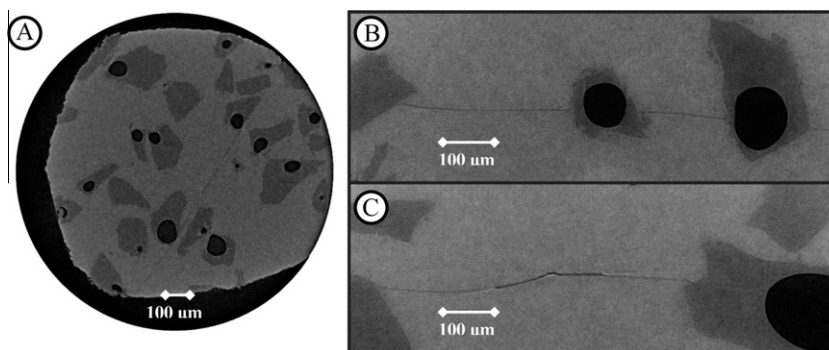


Fig. 1. (A) Low magnification Xum images of EMAA particles with bubbles dispersed in epoxy resin and (B and C) high magnification Xum images of healed SENB samples with cracks that are (B) completely filled and (C) partially filled with EMAA healing agent.

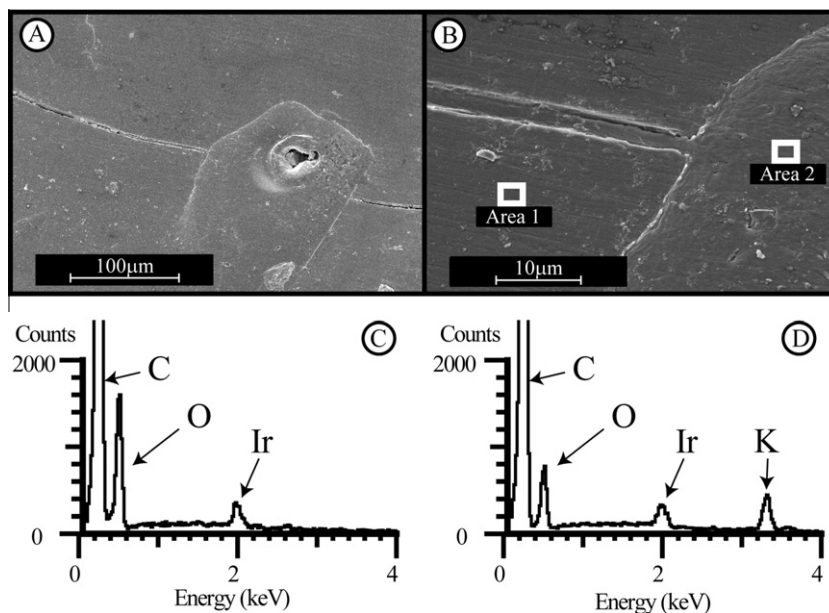


Fig. 2. (A) Low magnification SEM image of the polished cross-section of a healed SENB sample with the crack perpendicular to the sample surface, (B) high magnification SEM image of the polished cross-section of a healed SENB with the crack perpendicular to the sample surface showing the areas scanned with EDS, (C) EDS scan result from Area 1 showing only carbon, oxygen and the iridium coating peaks and (D) EDS scan result from Area 2 showing the carbon, oxygen, iridium coating and potassium peaks.

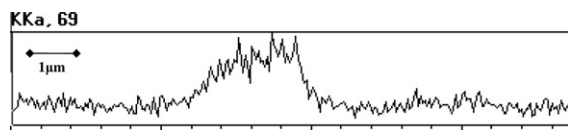


Fig. 3. EDS line scan result across a polished cross-section of a healed SENB for potassium showing that potassium is found exclusively in the crack plane filled by EMAA and not the epoxy matrix.

phase, the high magnification SEM image revealed that some of the EMAA had flowed into the crack plane during healing. An EDS line scan across a rejoined section of the crack as shown in Fig. 3 revealed that potassium was present inside the crack but not on either of the adjacent sides of the crack. This again shows that EMAA had flowed into the crack during healing and rejoined the adjacent resin fracture surfaces in the resin.

A 3D rendered Xum shown in Fig. 4 illustrates another aspect of the pressure delivery or bubble expansion mechanism. Bubble expansion within the EMAA particles are clearly observed to be larger when situated adjacent to the crack plane (indicated by white line) compared to those far away from the damage zone. This confirms that the bubbles within the EMAA can only expand (and hence push the EMAA) into a crack plane, when there is a cavity or space available, highlighting the mechanisms selectivity. While the precise cause of the formation and growth of the bubbles is not known, FTIR studies [24] have shown that a variety of reactions between the EMAA and epoxy resin during the post-cure phase produce volatiles. Indeed Fig. 5 presents an SEM image of an epoxy and EMAA interface after post-cure at 150 °C showing a highly porous

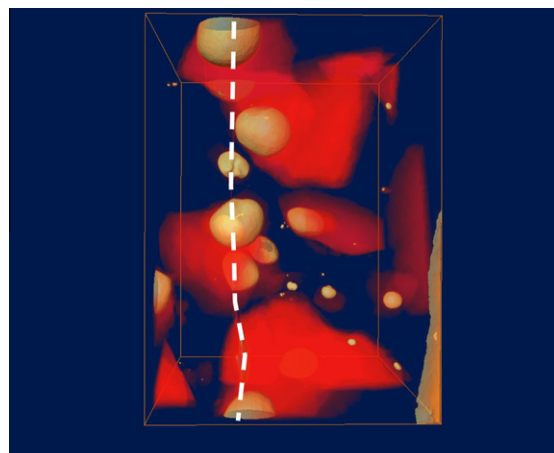


Fig. 4. Rendered 3D image of the mendable resin after healing, showing the increased sizes of the bubbles in the EMAA adjacent to the crack plane with the smaller sized bubbles further from the crack plane.

structure. The porosity observed is attributed to the phase separation of volatile products, such as water, which ultimately are able to form the bubbles providing the latent pressure delivery mechanism. It is also worth noting that long term effectiveness of the healing agent is dependent upon the volatiles which remain encapsulated within the thermoplastic indefinitely, as diffusion out of the thermoplastic would reduce the ability of the pressure delivery mechanism to operate. Hence both Xum and SEM confirm the proposed healing mechanism takes place in the mendable resins contain EMAA.

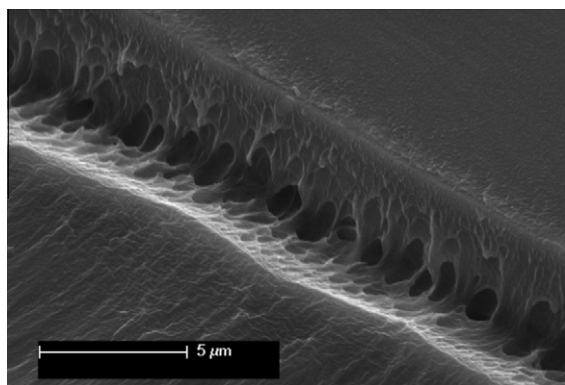


Fig. 5. SEM image of the epoxy EMAA interface after post-cure showing the highly porous interface and origin of the volatile species which ultimately produce the bubbles within the EMAA particle.

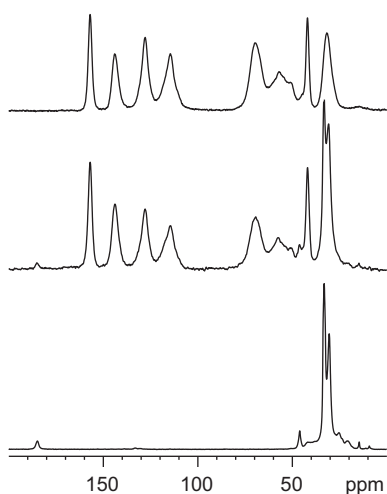


Fig. 6. NMR spectra of unmodified resin (top), mendable resin (middle) and EMAA (bottom).

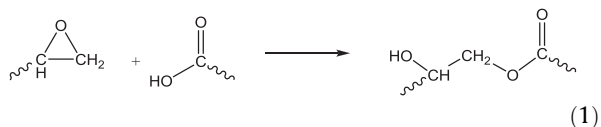
3.2. Investigation of the chemistry of healing

The solid state NMR of the EMAA, unmodified resin and mendable resin were collected and shown in Fig. 6. The spectrum of the mendable polymer appears as the sum of the EMAA and resin components, indicating that both components remain largely unchanged. The peak near 180 ppm in the mendable resin indicates that the acid functionality of the EMAA remains largely unreacted during curing of the mendable resin. This would be expected if the EMAA remained as a discrete phase during curing. NMR spectroscopy has therefore revealed that the cured mendable resin possesses the functionality needed for the proposed healing mechanism to take place.

Binding interactions between the EMAA and cured epoxy resin were assessed using butt joints possessing a range of functional group concentrations. Butt joints were selected for use over other adhesion testing methods because the high testing speeds used promote adhesive fail-

ure rather than cohesive failure. By promoting adhesive failure in the joint, the peak load sustainable in butt joints best reflects the strength of the EMAA–epoxy interface such that varying the oxirane, amine and hydroxyl group concentrations can be used to identify interactions binding the EMAA and resin together during healing. This study utilised the effect of post-cure time at 150 °C on functional group concentration in epoxy resins to vary the oxirane, amine and hydroxyl group concentrations in butt joint test pieces. To do this, peak intensities obtained from mid and near infrared spectroscopy were used to monitor the oxirane (915 cm⁻¹ peak), amine (6500–6650 cm⁻¹ peak [30]) and hydroxyl (7000 cm⁻¹ peak) group concentrations in the resin (Fig. 7). Binding interactions between EMAA and the cured resin were then identified from trends in butt joint strength with respect to the changes in functional group concentration.

Comparison of the changes in adhesive strength during post-cure (Fig. 8) with the changes in amine and oxirane concentration, suggest that acid–oxirane and/or acid–amine reactions (Eqs. (1) and (2)) provide the greatest strength to the EMAA–epoxy binding mechanism than any other.



For example, at short post-cure times, from 0–5 min, a small decrease in adhesive strength (from 6.4 to 5.3 kPa), is observed which compares with a modest decrease in oxirane and amine functional groups concentration. Furthermore at longer post cure times of ≥10 min, where the oxirane or amine concentrations are becoming depleted, the adhesive strengths (1.6–2.2 kPa) decrease substantially. While significantly lower than the initial adhesive strength of 6.4 kPa, the adhesive strength value of 1.6 kPa determined after 30 min of post curing at 150 °C indicates that significant binding between EMAA and cured resin still takes place despite the negligible levels of unreacted oxirane and amine groups. While providing insight into the binding reactions, which are critical to the formation of the pressure delivery mechanism, these results also provide critical information relating to the ultimate level of healing in the absence of functional groups. This adhesion can therefore be attributed to the formation of hydrogen bonding between acid groups in the EMAA and hydroxyl, tertiary amine and ether groups contained within the crosslinked polymer network. Given that the self-healing epoxy is made using stoichiometric reagent ratios and is post cured at 150 °C for 30 min (resulting in an epoxy containing low concentrations of oxirane and primary/secondary amine groups) hydrogen bonding is therefore likely to be the dominant bonding mechanism during the healing process in the EMAA–epoxy system. Despite this, the discovery that resins containing unreacted amine

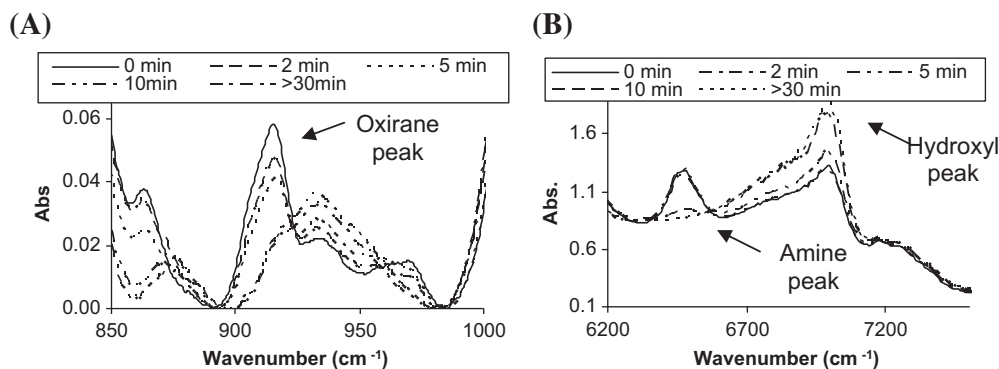


Fig. 7. (A) ATR-FTIR and (B) NIR spectra of butt joint test pieces with varying post cure times at 150 °C.

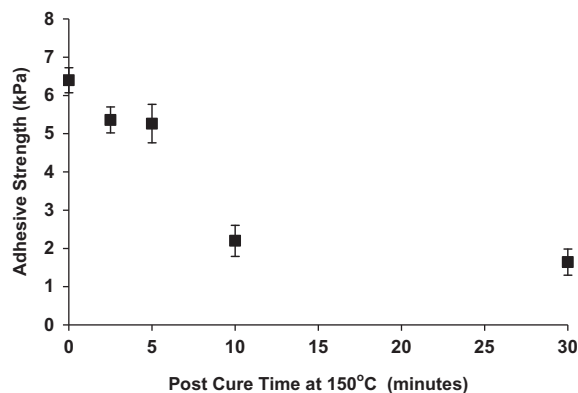


Fig. 8. Adhesive strength of epoxy resin butt joints joined with EMAA film with respect to post-curing time at 150 °C.

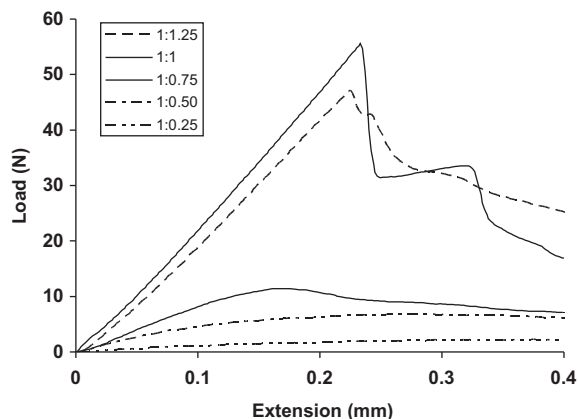
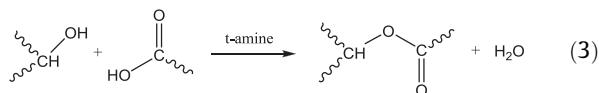


Fig. 9. Load versus extension plots of healed mendable resins made with different oxirane:amine ratios.

and/or oxirane functional groups have significantly higher adhesive strengths, can be used to improve the healing efficiency of thermoplastic additive based self healing systems in the future.

The importance of the binding reactions to the particle–matrix interface is further examined by varying the epoxy amine stoichiometry of the mendable resin and evaluating the effect upon healing using SENB methods. Fig. 9 shows that healing efficiency decreased sharply when the formulation went from a stoichiometric blend to one that contained an excess oxirane functional groups. This is despite the increased concentration of oxirane groups available for bonding to the EMAA particles and the above discussion, which suggests that increased oxirane groups should produce improved adhesion. SEM imaging however, reveals differences between the fracture surfaces of an excess oxirane blend and a stoichiometric ratio in Fig. 10A and B, respectively. The excess oxirane formulation displayed no bubbles surrounding or within EMAA at all, while the stoichiometric oxirane:amine formation revealed the formation of bubbles both in the particle and at the particle–matrix interface. This shows that that healing occurred via the pressure delivery mechanism for the stoichiometric formulation, while being restricted to particle healing only for the excess oxirane formulation.

The large decrease in load recovery after healing, for the excess oxirane formulation, illustrates the role of the interfacial reactions occurring between the EMAA particles and the epoxy matrix to the healing mechanism. Importantly, Meure et al. [24] have shown in FTIR studies that without the catalytic effect of the tertiary amine formed during oxirane amine reaction, the acid hydroxyl reaction (Eq. (3)) does not readily occur.



Given that the acid/amine reaction (Eq. (2)) has been shown to be unlikely to occur in typical healing conditions [24], the acid/hydroxyl reaction (Eq. (3)) is therefore necessary to produce the volatiles which ultimately facilitate the pressure delivery healing mechanism. In this example, tertiary amines can form via the oxirane and amine reaction and thus facilitate the operation of Eq. (3). It is proposed that for stoichiometric and excess amine formulations, tertiary amine is produced in sufficient concentrations to allow the acid/hydroxyl (Eq. (3)) to proceed, and therefore facilitating the healing mechanism. However, for excess epoxy formulations, insufficient tertiary amine would be

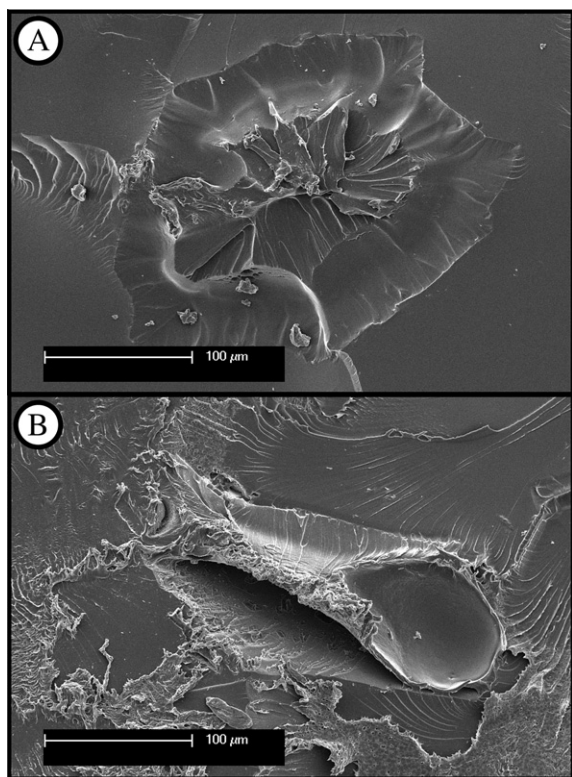


Fig. 10. SEM image of healed SENB fracture surfaces of mendable resins with (A) excess oxirane and (B) stoichiometric oxirane:amine ratio.

produced to catalyse the acid/hydroxyl reaction (Eq. (3)) and deleteriously compromising the pressure delivery mechanism.

4. Conclusions

This work has confirmed the healing mechanism of a mendable epoxy resin to consist of the pressure delivery of the EMAA thermoplastic into a crack plane during thermal activation. The pressure originates from the formation of a bubble within the EMAA thermoplastic due to interfacial reactions between the epoxy and EMAA producing volatiles during post-cure. During healing at elevated temperature, the internal pressure rises within this bubble as the volatiles expand and if the healing temperature is above the melting point of the thermoplastic, the healing agent is able to be pushed into an available cavity. X-ray ultra-microscopy (Xum), scanning electron microscopy (SEM) and energy dispersive spectroscopy (EDS) were all able to provide evidence for volatile formation, bubble expansion and delivery of the healing agent. The interfacial reactions between epoxy and EMAA during post-cure, have been correlated with adhesive and fracture toughness measurements, and highlight the importance of the type of bonding to the overall healing mechanism. The hydroxyl acid reaction (catalysed via tertiary amine groups) from the epoxy matrix and EMAA, respectively was shown to be critical during post-cure as it produced the volatiles which ultimately formed the bubbles necessary for the

pressure delivery mechanism. This was confirmed through comparisons between FTIR spectroscopy and SENB fracture toughness measurements. After healing however, FTIR spectroscopy and adhesion measurements showed that hydrogen bonding was likely to be the dominant adhesion mechanism which was responsible for the re-binding of the crack interface.

References

- [1] Hayes SA, Jones FR, Marshiya K, Zhang W. A self-healing thermosetting composite material. *Compos A Appl Sci Manuf* 2007;38(4):1116–20.
- [2] Wu DY, Meure S, Solomon D. Self-healing polymeric materials: a review of recent developments. *Prog Polym Sci* 2008;33(5):479–522.
- [3] Wool RP. Self-healing materials: a review. *Soft Matter* 2008;4(3):400–18.
- [4] Bergman SD, Wudl F. Mendable polymers. *J Mater Chem* 2008;18(1):41–62.
- [5] Murphy EB, Wudl F. The world of smart healable materials. *Prog Polym Sci* 2010;35(1–2):223–51.
- [6] Caruso MM, Blaszik BJ, White SR, Sottos NR, Moore JS. Full recovery of fracture toughness using a nontoxic solvent-based self-healing system. *Adv Funct Mater* 2008;18(13):1898–904.
- [7] White SR, Sottos NR, Geubelle PH, Moore JS, Kessler MR, Sriram SR, et al. Autonomic healing of polymer composites. *Nature* 2001;409(6822):794–7.
- [8] Rong MZ, Zhang MQ, Zhang W. A novel self-healing epoxy system with microencapsulated epoxy and imidazole curing agent. *Adv Compos Lett* 2007;16(5):167–72.
- [9] Xiao DS, Yuan YC, Rong MZ, Zhang MQ. Hollow polymeric microcapsules: preparation, characterization and application in holding boron trifluoride diethyl etherate. *Polymer* 2009;50(2):560–8.
- [10] Wang HP, Yuan YC, Rong MZ, Zhang MQ. Microencapsulation of styrene with melamine-formaldehyde resin. *Colloid Polym Sci* 2009;287(9):1089–97.
- [11] Trask RS, Williams GJ, Bond IP. Bioinspired self-healing of advanced composite structures using hollow glass fibres. *J R Soc Interface* 2007;4(13):363–71.
- [12] Pang JWC, Bond IP. 'Bleeding Composites' – damage detection and self-repair using a Biomimetic Approach. *Compos A Appl Sci Manuf* 2005;36(2):183–8.
- [13] Williams GJ, Bond IP, Trask RS. Compression after impact assessment of self-healing CFRP. *Compos A Appl Sci Manuf* 2009;40(9):1399–406.
- [14] Williams HR, Trask RS, Knights AC, Williams ER, Bond IP. Biomimetic reliability strategies for self-healing vascular networks in engineering materials. *J R Soc Interface* 2008;5(24):735–47.
- [15] Trask RS, Bond IP, Williams GJ, Williams HR. Bioinspired self-healing of advanced composite materials. Schaumburg, IL, United States: American Institute of Aeronautics and Astronautics Inc., Reston, VA 20191-4344, United States; 2008. p. 2008–864.
- [16] Chen XX, Wudl F, Mal AK, Shen HB, Nutt SR. New thermally remendable highly cross-linked polymeric materials. *Macromolecules* 2003;36(6):1802–7.
- [17] Murphy EB, Bolanos E, Schaffner-Hamann C, Wudl F, Nutt SR, Auad ML. Synthesis and characterization of a single-component thermally remendable polymer network: Staudinger and Stille revisited. *Macromolecules* 2008;41(14):5203–9.
- [18] Rule JD, Sottos NR, White SR, Moore JS. The chemistry of self-healing polymers. *Educ Chem* 2005;42(5):130–2.
- [19] Wudl F, Chen X. Thermally re-mendable crosslinked polymers, monomers, their manufacture, and thermally mending. Application US: The Regents of The University of California, USA; 2004. p. 32.
- [20] Wood A. Polymer, heal thyself. *Chem Week* 2002;164(10):31.
- [21] Hayes SA, Zhang W, Branthwaite M, Jones FR. Self-healing of damage in fibre-reinforced polymer-matrix composites. *J R Soc Interface* 2007;4(13):381–7.
- [22] Meure S, Wu DY, Furman S. Polyethylene-co-methacrylic acid healing agents for mendable epoxy resins. *Acta Mater* 2009;57(14):4312–20.
- [23] Meure S, Wu DY, Furman S. Identification of critical conditions for healing in a mendable EMAA-Epoxy Resin. *Compos Sci Technol*; in press, doi:10.1016/j.compscitech.2011.12.007.

- [24] Meure S, Wu DY, Furman S. FTIR study of bonding between a thermoplastic healing agent and a mendable epoxy resin. *Vib Spectrosc* 2010;52(1):10–5.
- [25] Meure S, Furman S, Khor S. Poly[ethylene-co-(methacrylic acid)] healing agents for mendable carbon fiber laminates. *Macromol Mater Eng* 2010;295(5):420–4.
- [26] Mayo SC, Davis TJ, Gureyev TE, Miller PR, Paganin D, Pogany A, et al. X-ray phase-contrast microscopy and microtomography. *Opt Express* 2003;11(19):2289–302.
- [27] Gureyev TE. X-TRACT Web site. 2008.
- [28] Paganin D, Mayo SC, Gureyev TE, Miller PR, Wilkins SW. Simultaneous phase and amplitude extraction from a single defocused image of a homogeneous object. *J Microsc Oxford* 2002;206:33–40.
- [29] Coleman MM, Lee JY, Painter PC. Acid salts and the structure of ionomers. *Macromolecules* 1990;23(8):2339–45.
- [30] Chabert B, Lachenal G, Tung CV. Epoxy-resins and epoxy blends studied by near-infrared spectroscopy. *Macromol Symp* 1995;94:145–58.